Azab, Mohamed

Article

Multi-objective design approach of passive filters for single-phase distributed energy grid integration systems using particle swarm optimization

Energy Reports

Provided in Cooperation with:
Elsevier

Suggested Citation: Azab, Mohamed (2020) : Multi-objective design approach of passive filters for single-phase distributed energy grid integration systems using particle swarm optimization, Energy Reports, ISSN 2352-4847, Elsevier, Amsterdam, Vol. 6, pp. 157-172, https://doi.org/10.1016/j.egyr.2019.12.015

This Version is available at:
https://hdl.handle.net/10419/244022

Energy Reports 6 (2020) 157–172

Contents lists available at ScienceDirect

Energy Reports

journal homepage: www.elsevier.com/locate/egyr

Research paper

Multi-objective design approach of passive filters for single-phase distributed energy grid integration systems using particle swarm optimization

Mohamed Azab

EEET Department, Faculty of Engineering, Benha University, Egypt
EEET Department, Yanbu Industrial College, KSA

ARTICLE INFO

Article history:
Received 8 September 2019
Received in revised form 2 December 2019
Accepted 17 December 2019
Available online 30 December 2019

Keywords:
Distributed energy resources
Grid connected inverter
Grid integration
Passive filter
Particle swarm
Optimization techniques
Evolutionary computation
Fuel cell
Photovoltaic
Batteries

ABSTRACT

This article presents a non-conventional design approach of high order passive filters incorporated with distributed energy grid integration systems based on particle swarm optimization (PSO) as one of multi-objective evolutionary search algorithms. Two topologies of passive grid filters (third order passive damped LCL-filter and trap filter) are chosen as case studies. The presented grid filter design is based searching the optimum values of filter passive elements that can optimize an objective function composed of several terms such as harmonic attenuation factor and size (value) of passive elements (inductors and capacitors). The employed multi-objective design approach has three main advantages: (1) The PSO algorithm offers several groups of solutions to the same optimization problem. Accordingly, the most convenient solution can be chosen based on several factors such as cost of realization, availability in the market and the corresponding THD of grid current. (2) Multi-objective design approach is flexible enough to include other factors in the customized objective function to achieve different design criteria in accordance with new (or updated) versions of grid codes. (3) The PSO algorithm converges to the optimum solution(s) regardless the initial search values (initial guess). Consequently, the algorithm does not need any prior knowledge about filter numerical values

The PSO algorithm has been developed in Matlab®, while the overall hardware grid-integration system has been modeled and studied using PSIM® software package. The obtained results demonstrate the effectiveness of the proposed approach to get practical and applicable values of filter components that result in good harmonic attenuation and satisfy the related codes of grid integration such as the IEEE standard 519.

The main contribution of this paper is the utilization of evolutionary optimization technique to achieve an optimum design of passive grid filters that can optimize simultaneously several contradictory goals such as achieving the maximum possible harmonic attenuation at the lowest possible filter size. Compared with conventional design approach, the PSO-based filter design approach results in lower numerical values of filter components, which leads to considerable reduction in the size and cost of the passive grid filter. Moreover, grid filter design based on evolutionary search approach permits accommodation of several design criteria in the customized objective function with arbitrary weighting factors upon system design requests and new grid codes constrains.

1. Introduction

Grid integration systems with Distributed Energy Resources (DER) gained increasing importance during the last decade. Several schemes have been adopted for single-phase and three-phase systems. The core power components of typical grid integration system are the grid-tied inverter and the passive grid filter. In case of low power residential systems a current controlled two-level inverter is commonly utilized as a power conditioner, while in case of three-phase DER systems, multilevel inverter is preferable especially for high power applications where the switching frequency is relatively low. Utilization of such systems, injects to the electric grid unwanted current harmonics produced by the inverter that degrade the system performance. Therefore, many standards such as IEEE-519 and IEEE-1547 have been developed to restrict the injection of undesired harmonics to the grid (Jayalath and Hanif, 2018; Anzalchi et al., 2017; Beres, 2016). Accordingly, in all power ranges, low pass filter is necessary to be inserted between the grid-tied inverter and the grid in order to

E-mail address: mohamed.ahmed.azab@ieee.org.

https://doi.org/10.1016/j.egyr.2019.12.015

satisfy the requirements of such related standards (Anzalchi et al., 2017).

Optimum design of passive filter for grid integration systems is not a trivial task due to several factors such as possible resonance between passive filter and grid impedance (Beres, 2016; Fang et al., 2017b). Optimum filter design that meets the aforementioned standards at low possible cost is a challenging issue that cannot be guaranteed by conventional design procedure with traditional simple first order L-filter (Li et al., 2015). Consequently, high order topologies of passive filter can provide better harmonic attenuation at lower value of total inductance, which decreases the size and cost of the filter (Chayjani and Monfared, 2016b).

1.1. Objectives of the article

The main objective of this article is to provide a non-conventional design approach of high order passive filters (inserted between grid-connected inverter and the electric grid) based on PSO technique. The PSO algorithm (developed in Matlab®) aims to find the optimum values of passive filter elements that can satisfy some criteria such as maximum possible harmonic attenuation at minimum possible size of filter elements (L and C).

The papers aims to apply and study the non-conventional design approach (based on PSO) on two schemes of passive grid filters: Passive damped LCL filter (L-RC-L) scheme shown in Fig. 3d and Trap filter (LLCL) scheme shown in Fig. 3e.

Moreover, the paper assesses and performs qualitative and quantitative analysis to the PSO obtained solutions of passive filter by plugging the filter numerical values into a hardware model of single-phase DER grid integration system developed in PSIM® simulation package. In addition, comparison with conventional design approach has been conducted as well.

The rest of the paper is organized as follows. Section 2 addresses the location and different topologies of passive grid filters. Section 3 describes the investigated system. Section 4 discusses the design criteria of passive grid filters. Section 5 presents the PSO technique. Section 6 investigates the design procedure of passive grid filter using PSO techniques and presents also the obtained results. Section 7 demonstrates the comparison with conventional design approach. Section 8 is the conclusion of the paper. Section 9 is assigned to references. While Appendix includes a group of appendices.

2. Passive grid filters

2.1. Location of filter with respect to grid integration system

A typical single-phase DER grid integration system is illustrated in Fig. 1, where multiple energy resources (PV and FC) are connected to a common dc bus of 400 V. Each resource is incorporated with its own power conditioner (dc–dc converter) to control the output voltage to the desired value of the dc bus. The produced energy is injected to the electric grid through single-phase grid-tied inverter usually working in current controlled mode (Azab, 2017; Chayjani and Monfared, 2016; Sharma and Goel, 2017). Due to the harmonics injected from the PWM inverter, the passive grid filter is connected between the inverter outputs and the electric grid to attenuate the high frequency harmonics injected to the grid and restrict the low order harmonics to permissible level in accordance with the grid codes and standards such as IEEE-519 standard (Jayalath and Hanif, 2018; Anzalchi et al., 2017; Beres, 2016; Fang et al., 2017b,c; Li et al., 2015; Chayjani and Monfared, 2016b).

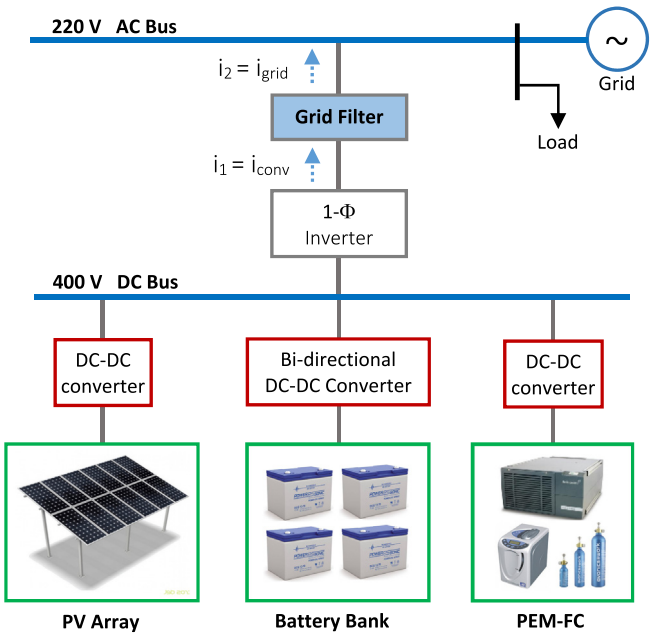

Fig. 1. Single line diagram of the investigated DER grid integration system.

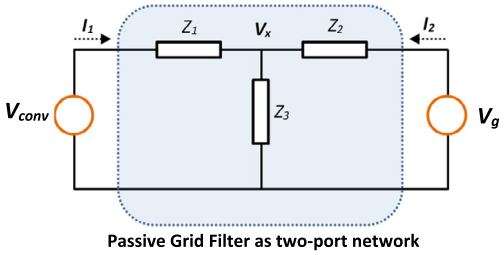

Fig. 2. Generalized scheme of passive grid filter.

2.2. Generalized scheme of passive grid filter

Many existing schemes of passive filters can be employed with DER grid integration systems. Each scheme has its distinct characteristics and features (Beres, 2016; Chayjani and Monfared, 2016; Xu et al., 2014). Fortunately, a passive grid filter can be represented by a generalized topology as shown in Fig. 2. By configuring the filter impedances (Z_1, Z_2 and Z_3) several topologies can be achieved. The commonly used schemes in grid integration systems are L, LR filters and LCL with a damping resistor as illustrated in Fig. 3.

2.3. Commonly used schemes of passive grid filter

In addition, many other emerging schemes of high order filters have been reported such as trap filter (Fang et al., 2017b), LTCL (Fang et al., 2017c) and LCL-LC filters (Li et al., 2015) that can provide better harmonic attenuation and lower size of filter components (Fang et al., 2017a). Multi-tuned trap filter is presented as well in Chayjani and Monfared (2016b) where selected harmonics are bypassed by the LC-traps and blocked from injection to the electric grid (Chayjani and Monfared, 2018; Xu et al., 2014).

According to Fig. 2, the generalized filter transfer functions (I_2/V_{conv}) and (I_2/I_1) can be derived by considering the grid filter as Two-Port Network and determining some Y-model parameters and h-model Parameters.

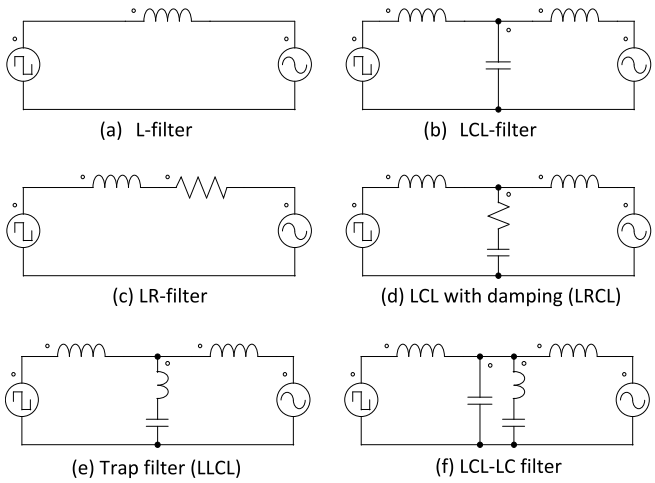

Fig. 3. Different topologies of passive grid filters.

The general formula of $I_2(s)/V_{conv}(s)$ and $I_2(s)/I_1(s)$ are described by Eqs. (1) and (2) respectively. The detailed mathematical derivation of those equations is presented in Appendix A.1.

$$Y_{21} = \frac{I_2(s)}{V_{conv}(s)} = \frac{Z_3}{Z_1Z_2 + Z_2Z_3 + Z_1Z_3} \tag{1}$$

$$h_{21} = \frac{I_2(s)}{I_1(s)} = \frac{Z_3}{Z_2 + Z_3} \tag{2}$$

Different filter topologies can be achieved by configuring the impedances (Z_1, Z_2 and Z_3) to specific passive elements as summarized in Table 1. The corresponding circuit diagram of such filter schemes are shown in Fig. 3, while the corresponding filter transfer functions Y_{21} and h_{21} are derived and summarized in Table 1.

In this article, two filter schemes have been investigated: LCL with damping resistor (LRCL) and LLCL trap filter.

3. Grid-integrated system under investigation

3.1. Description of the system

A circuit diagram of the investigated system and the inverter control system are shown in Fig. 4a and b respectively. The common DC bus of the DER grid integration system is illustrated in Fig. 4c. The employed single-phase grid-integrated system can be divided into three major sections:

(1) Distributed energy resources (PV Array, PEM FC, and Battery Bank) that are connected together through proper power electronic conditioners (step up dc–dc converters) forming a common DC bus of 400 V as illustrated in Fig. 4a.
(2) Single-phase grid-tied inverter whose DC inputs are fed from the DER through the common DC bus.
(3) Passive filter inserted between the inverter and the electric grid to satisfy grid integration requirements.

The employed DER system is formed by: 5.12 kWP PV array, 4.8 kW PEM FC modules, 120 V/100 AH Battery Bank. Each resource is incorporated with a boost dc–dc converter to raise and control the output voltage of PV array and PEM-FC to 400 V to form a fixed DC bus voltage. While the battery bank is connected to the DC bus through a bidirectional converter such that the battery bank can inject its power to the grid (discharging mode: dc–dc converter is working in step up mode) or it can be charged from the PV array or from the PEM FC (charging mode: dc–dc converter is working in step down mode).

The investigated system represents a typical residential application of renewable energy grid-tied system (Xu et al., 2013; Li et al., 2018b; Azab, 2019, 2018). Details of the items' specifications and simulation parameters are presented in Appendix A.3.

The study is conducted on two schemes of grid passive filters are: LCL filter with a damping resistor (L-RC-L) scheme (Fig. 3d) and Trap filter (LLCL) scheme (Fig. 3e). The optimum values of grid filter components determined by the PSO search algorithm (described later in Section 4) are plugged into the overall system model illustrated in Fig. 4a and c. The common dc bus voltage (400 V system) is controlled via three independent power optimizers (dc–dc converters). The dc bus voltage is described by the following relations:

$$V_{DC} = \frac{V_{PV}}{1 - d_{pv}} \tag{3a}$$

$$V_{DC} = \frac{V_{FC}}{1 - d_{fc}} \tag{3b}$$

When the battery bank is injecting power to the dc bus (discharging mode) the bidirectional dc–dc converter is working in step up mode (boost converter) such that the dc bus voltage is given also by Eq. (4a).

$$V_{DC} = \frac{V_{BAT}}{1 - d_{bat}} \tag{4a}$$

If the battery is charging from the PV or from the FC modules (charging mode), the bidirectional dc–dc converter is working in step down mode (buck converter) such that the battery bank voltage is given by Eq. (4b):

$$V_{BAT} = d_{bat} V_{DC} \tag{4b}$$

where V_{PV} is voltage of PV array, V_{FC} is the voltage of FC modules and V_{BAT} is the dc voltage of the battery bank. As the dc voltage produced by the DER: PV array, FC modules and Battery bank are not equal, the corresponding power optimizer (dc–dc converter) is operating at its own duty cycle whose value is limited between safe minimum and maximum values [0.2,0.8] such that:

$$d_{pv} \neq d_{fc} \neq d_{bat} \tag{5a}$$

$$\begin{cases} 0 < d_{pv} < 1 \\ 0 < d_{fc} < 1 \\ 0 < d_{bat} < 1 \end{cases} \tag{5b}$$

In case of PV array, the duty cycle (d_{pv}) of the PV converter is generated from a MPPT unit based on the well know method (P&O). While the duty cycle (d_{fc}) of the FC converter is generated

Table 1
Transfer functions of different topologies of passive grid filter.

		Impedances			Transfer Functions	
		Z_1	Z_2	Z_3	$\frac{I_2(s)}{V_1(s)}$	$\frac{I_2(s)}{I_1(s)}$
Filter Scheme	L	SL_1	0	∞	$\frac{1}{SL_1}$	1
	LR	$SL_1 + R$	0	∞	$\frac{1}{(SL_1 + R)}$	1
	LCL	SL_1	SL_2	$\frac{1}{SC}$	$\frac{1}{S^3L_1L_2C + S(L_2+L_1)}$	$\frac{1}{S^2L_2C + 1}$
	L-RC-L	SL_1	SL_2	$R + \frac{1}{SC}$	$\frac{(SCR + 1)}{S^3L_1L_2C + S^2RC(L_2+L_1) + S(L_2+L_1)}$	$\frac{SCR + 1}{S^2L_2C + SCR + 1}$
	TRAP	SL_1	SL_2	$SL_t + \frac{1}{SC_t}$	$\frac{(S^2C_tL_t + 1)}{S^3C_t(L_1L_2 + L_2L_t + L_1L_t) + S(L_2+L_1)}$	$\frac{(S^2C_tL_t + 1)}{S^2C_t(L_2 + L_t) + 1}$
	LCL-LC	SL_1	SL_2	$\left(SL_t + \frac{1}{SC_t}\right) \parallel \frac{1}{SC}$	$\frac{(S^2C_tL_t + 1)}{a_5S^5 + a_3S^3 + a_1S}$	$\frac{(S^2C_tL_t + 1)}{a_4S^4 + a_2S^2 + 1}$

LCL-LC filter: $a_1 = L_1 + L_2$; $a_2 = L_t C_t + L_2 (C + C_t)$; $a_3 = L_1 L_2 (C + C_t) + L_t C_t (L_1 + L_2)$; $a_4 = L_t C_t L_2 C$; $a_5 = L_1 L_2 L_t C_t C$;

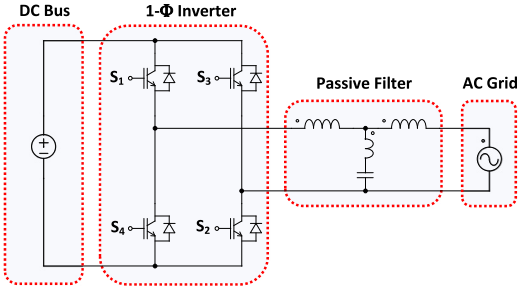

4a.Simplified circuit diagram

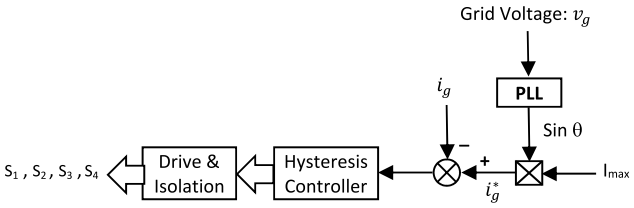

4b.Block diagram of Inverter control unit

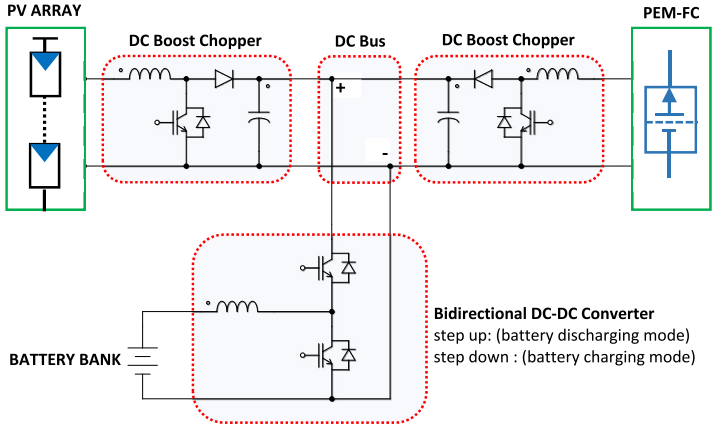

4c. Circuit diagram of common DC Bus of DER

Fig. 4. Configuration of the investigated grid-tied system.

based on a closed loop control of the dc bus voltage using PI controller. Similarly, the duty cycle (d_{bat}) is produced from a closed loop PI controller. The details of MPPT unit and the dc bus voltage control is out of scope of this article.

3.2. System rating and base values

The system rating is selected based on the assumption that the investigated grid integration system is intended for residential applications. Accordingly, the corresponding base values are calculated. The rated active power to be injected to the grid

Table 2
System rating and base values.

Parameter	Symbol	Value
Grid frequency	f_g	50 Hz
Supply voltage	V_g	220 V
Rated active power	P_{rated}	4 kW
Base frequency	f_B	50 Hz
Base voltage	V_B	220 V
Base impedance	Z_B	12.1 Ω
Base inductance	L_B	38.5 mH
Base capacitance	C_B	263.2 μF

is selected to be 4 kW. The grid voltage is 220 V/50 Hz. The maximum dc link voltage is 400 V, the maximum inverter switching frequency is 10 kHz. Thus, the base values of impedance, capacitance and inductance are computed using Eqs. (6a)–(6c) respectively. The system rating and the computed base values are summarized in Table 2.

$$Z_B = \frac{V_B^2}{P_{rated}} \tag{6a}$$

$$C_B = \frac{1}{\omega_B Z_B} \tag{6b}$$

$$L_B = \frac{Z_B}{\omega_B} \tag{6c}$$

4. Design criteria of passive grid filters

4.1. Conventional/systematic design

In general, design methodologies of grid filters aim to achieve a major objective of satisfying the grid codes and standards requirements by attenuating high order current harmonics injected to the grid to specific safe levels determined by the related standards. Conventional filter design criteria aim to take into consideration the following factors in order to determine the suitable rating of the passive components:

1. Maximum grid-side current ripple: it should not exceed an upper limit (Chayjani and Monfared, 2016).
2. Maximum inverter-side current ripple: it should not exceed an upper limit (Mahamat et al., 2017).
3. Resonant frequency range (Wu et al. 2012): it is governed by the rule: $(10f_g < f_{res} < 0.5f_{swt})$ (7)
4. Damping at resonance frequency: it should be employed either by damping resistor R (passive damping) or active damping (control algorithm).
5. Limited capacitive reactive power Q_c: to be a small percentage of nominal rated power (Chayjani and Monfared, 2016; Li et al., 2015; Mahamat et al., 2017).

4.2. Multi-objective design criteria

Recently, design of high order grid filters aims to achieve other objectives such as minimization of size and weight of passive filter (Li et al., 2018a) (due to space and volume restrictions) and minimization of filter overall cost. Besides that, minimization of filter inductance based on maximum permissible THD as performance index (Anzalchi et al., 2016). Such multi-objectives features of filter design are summarized below:

1. Minimum size and weight: achieved by minimization of the total inductance and the size of capacitor C.
2. Minimum power losses across the damping resistor R (Ye et al., 2018) that can be achieved by minimizing the current that flows in the damping resistor branch (maximizing the R).
3. Minimum overall stored energy in the filter:
$$\left(E_L = \frac{1}{2}LI^2, E_C = \frac{1}{2}CV^2\right) \tag{8}$$

Unfortunately, some objectives are contradictory such as the contradiction between good harmonic attenuation and minimum size, weight of the filter. So, it is important to make a compromise between the parameters to get optimum values of filter components and achieve a satisfactory performance. Thus, evolutionary computational techniques would be efficient to get an optimum design that can take into consideration major objectives and prioritize the desired features of the filter based upon custom design request.

5. Evolutionary computational algorithms

5.1. Introduction

Many evolutionary computational algorithms have been developed and applied successfully in electrical engineering optimization problems (Azab, 2015; Singh and Singh, 2014; Tan, 2018). Some of well-known algorithms are: Ant Colony algorithm (ACO) (Liu et al., 2018; Zhang et al., 2019; Ma et al., 2019; Yin et al., 2018; Yang et al., 2019a), Biogeography-Based Optimization (BBO) (Al-Roomi and El-Hawary, 2019; Ma et al., 2017; Tegou et al., 2018; Sarker et al., 2018), Genetic Algorithms (GA) (Mohammadi et al., 2019; Corus and Oliveto, 2018; Han et al., 2018; Wang et al., 2018a) and Particle Swarm optimization (PSO) (Liu et al., 2019; Sebtahmadi et al., 2018; Liu et al., 2017; Ning et al., 2019; Lee et al., 2018; Leboucher et al., 2018; Yang et al., 2019b; Zhang et al., 2018; Wang et al., 2018b; Yang et al., 2018). Such techniques could solve a variety of complex engineering problems that are difficult to solve using traditional methods.

5.2. Particle swarm optimization (PSO)

PSO is an optimization technique that is capable of finding global optimal solution(s) by using social interaction of unsophisticated agents. In PSO, a flock of particles flies through a search space with velocity updated by movement inertia, self-cognition, and social interaction (Azab, 2015; Radosavljevic, 2018; Liu et al., 2019; Sebtahmadi et al., 2018; Liu et al., 2017). Initially, the particles are randomly placed in a search space of a certain problem or function. So, each particle represents a solution to the problem. An objective function is evaluated for each particle. Velocity and position of each particle is updated at each iteration by Eqs. (9) and (10) (Azab, 2015; Tan, 2018; Ning et al., 2019; Lee et al., 2018; Leboucher et al., 2018; Yang et al., 2019b; Zhang et al., 2018; Wang et al., 2018b; Yang et al., 2018).

$$v_i^{k+1} = wv_i^k + \alpha\left[L^k - x_i^k\right] + \beta\left[G^k - x_i^k\right] \tag{9}$$

$$x_i^{k+1} = x_i^k + +_i^{k+1} \tag{10}$$

where x_i is the position of the ith particle in the search space, v_i is the velocity of the ith particle, w is the inertia of particles, α & β are bounded positive uniformly distributed random vector. L is the particle's best position, G is the global best position found by all particles, k is the iteration number, i is the number of particles. Accordingly, the particles movement within the search space is affected by three factors: the previous movement of the same particle, the local best position of the same particle and the

Steps of the PSO Algorithm

1. **Initialization:** PSO parameters of optimization problem (L_1, L_2, C, R) are initialized randomly.
2. **Evaluation of initial solution:** The Objective Function is evaluated for all particles in the initial population (solution). The local best position L^k and global best particle, G^k are computed. Particle of the best objective function is chosen to be the global best particle for this first this iteration.
3. **Updating position and velocity**: The position x_i^{k+1} and the velocity v_i^{k+1} of particles are updated according to (9) and (10).
4. **New Evaluation of the updated solution:** The objective function is computed for the new position. (new solution). The local best position L^k and global best particle, G^k are updated as well.
5. **Repeat for all number of iteration:** The terminal condition (number of iterations reaching the maximum) or quality of the best solution being satisfactory. If the terminal condition has not been done, the process is repeated until the terminal condition is met.
6. **Output results:** The best solution of (L_1, L_2, C, R) obtained from the optimization process is determined.

Fig. 5. Summarized procedure of PSO algorithm.

best position obtained so far by any particle over the previous iterations (global best) (Singh and Singh, 2014). The procedure of PSO algorithm is shown in Fig. 5.

Owing to successful application of PSO technique in many optimization problems (Azab, 2015; Singh and Singh, 2014; Tan, 2018; Liu et al., 2019; Sebtahmadi et al., 2018; Liu et al., 2017; Ning et al., 2019; Lee et al., 2018; Leboucher et al., 2018; Yang et al., 2019b; Zhang et al., 2018; Wang et al., 2018b; Yang et al., 2018) it has been chosen among several evolutionary optimization techniques to solve the multi-objective optimization problem of grid filter design.

6. Design of passive grid filters using PSO

The PSO has been adopted to find an optimal design of two grid filter schemes: LCL with resistive damping and LLCL trap filter. The design approach is based on constrained iterative searching to the filter components that can satisfy specific objective function(s) of multiple terms (Aghajani and Ghadimi, 2018) and criteria as previously addressed in Sections 4.1 and 4.2.

6.1. Case 1: LCL filter with damping resistor (L-RC-L)

6.1.1. Formulation of multi-objective function

The circuit diagram of LCL filter with damping resistor is shown in Fig. 3d, while the corresponding transfer functions were presented in Table 1. Formulation of suitable objective function constitutes an essential part for successful algorithm. As given in Eq. (11), the objective function $J_{1\text{-}LCL}$ is elaborated to include three terms: harmonic attenuation, size of filter components and damping resistor. Therefore, the PSO algorithm searches for the optimum values of (L_1, L_2, C and R) that can achieve multiple objectives: (a) good harmonic attenuation (b) at minimum possible size of filter components (c) with maximum possible value of the damping resistor to ensure good damping at resonant frequency. The selection of passive components is restricted to resonant frequency constrain that should be within the range given by the inequality (7) that is re-written again in (12).

$$J_{1\text{-}LCL} = min\left[Y_{21\text{-}LCL} + \left(\frac{L_1 + L_2}{L_B} + \frac{C}{C_B}\right) + \frac{Z_B}{R}\right] \tag{11}$$

$$\text{Provided that:} \quad 10\, f_g < f_{res} < f_{max} \tag{12}$$

where ($Y_{21\text{-LCL}}$) is computed at maximum frequency ($f_{max} = 5$ kHz). Owing to the system base values presented in Table 2 the filter resonant frequency of the transfer function (Y_{21}) will be restricted by the inequality:

$$500\ \text{Hz} < f_{res} < 5000\ \text{Hz} \tag{13}$$

According to Eq. (11), minimum $Y_{21\text{-LCL}}$ contributes to good harmonic attenuation, minimum ($L_1 + L_2$) contributes to minimum inductor size, minimum (C) contributes to minimum size of capacitor and minimum (1/R) contributes to maximization of damping resistance (minimum current).

Table 3
Parameters of PSO Algorithm.

Parameter	Particles	Iterations	Inertia w	α β
Value	300	300	0.1	Random number [0–1]

Table 4a
Search space of estimated parameters of passive grid filter (LCL with damping resistor).

Parameter	L_1 (H)	L_2 (H)	C (F)	R (Ω)
Search space	0–1	0–1	0–1	0–100

Table 4b
Search space of estimated parameters of passive grid filter (trap filter).

Parameter	L_1 (H)	L_2 (H)	L_t (H)	C_t (F)
Search space	0–1	0–1	0–1	0–1

6.1.2. PSO parameters

The parameters of the elaborated PSO algorithm and the search space are presented in Tables 3 and 4 respectively. According to the presented values in Tables 4a and 4b the algorithm search space is wide which indicates that there is no restriction on the setting (selection) of the initial solution of the PSO algorithm unlike some algorithms which would have some restrictions and conditions on the initial guess values and sometimes trap in minimum local error points without reaching to a global optimum solution.

6.1.3. PSO obtained results

Actually, the PSO technique as one of powerful evolutionary computational method provides several advantages: 1. The obtained solution is not unique. i.e., there are many groups of solutions (non-unique solution) that can satisfy the objective

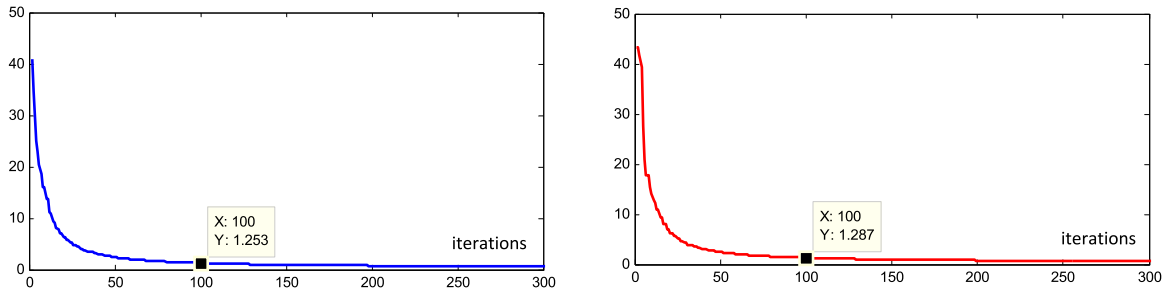

(a) Zero initial solution # 1 (b) Unity initial solution # 2

Fig. 6. Evolution of objective function $J_{1\text{-}LCL}$.

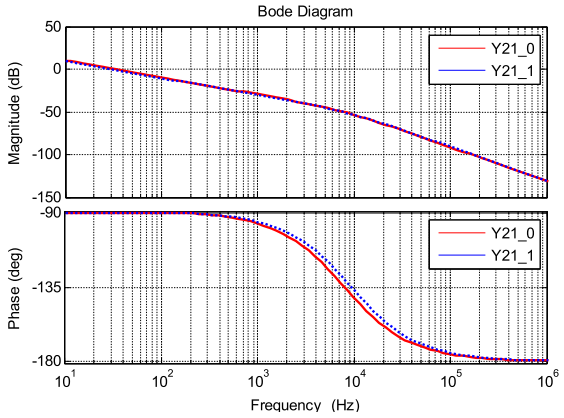

Fig. 7. Bode diagram of (L-RC-L) filter transfer function $Y_{21\text{-}LCL}$ for both groups of solutions Y_{21_0}: zero initial solution, Y_{21_1}: unity initial solution.

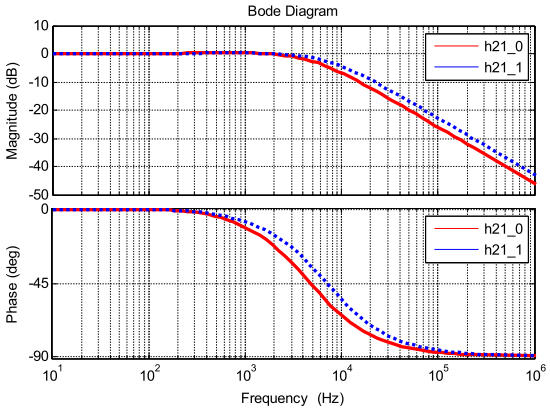

Fig. 8. Bode diagram of (L-RC-L) filter transfer function $h_{21\text{-}LCL}$ for both groups of solutions h_{21_0}: zero initial solution, h_{21_1}: unity initial solution.

function J_1 as presented in Table 5. Therefore, the designer is free to select the most applicable values of passive components that are easy to purchase or to fabricate.

2. The PSO algorithm converges to the solution(s) a part from the starting point (initial solution). In this work, the PSO initial solution was intentionally selected to be far from the possible real values to examine the robustness of the algorithm ($L_1 = L_2 = 0$ H, $C = 0$ F, $R = 0$ Ω). The PSO algorithm reaches successfully to satisfactory solutions after accepted number of iterations and relatively small CPU time (order of seconds) as presented in Table 5. Moreover, the PSO algorithm was tested with random values of initial solution and the program converged successfully also to a satisfactory solution. In addition, the PSO algorithm has been tested with unrealistic initial values of passive components ($L_1 = L_2 = 1$ H, $C = 1$ F, $R = 1$ Ω) as well. According to the obtained results the initial starting solution affects the initial value of the objective function and the required number of iterations to reach to the optimum solution (CPU time), but it has no effect on the algorithm divergence or trapping in minimum local errors as the case of Genetic Algorithm. It has also negligible effect on the final solution. As shown in Table 5, PSO evolutionary technique has found many solutions that lead to practical values of grid filter components.

According to Table 5, the deviation between the obtained solutions is small such that any of them can be utilized. Table (Li et al., 2015) presents some selected extreme optimum groups of solutions of L-RC-L filter obtained from the PSO algorithm for different initial solutions: zero initial conditions ($L_1 = L_2 = 0$, $C = 0$, $R = 0$) and unity initial conditions ($L_1 = L_2 = 1$, $C = 1$, $R = 1$) for zero and unity initial solutions. The extreme solutions mean that they satisfy minimum THD of grid current or minimum total inductance for cost reduction. Each group of

Table 5
Some PSO obtained solutions of (L-RC-L) filter.

Solution / Parameter	Zero initial solution			Unity initial solution		
	1	**2**	**3**	**1**	**2**	**3**
L_1 [H]	0.0028	0.0035	0.0031	0.0027	0.0021	0.0015
L_2 [H]	0.0018	0.0016	0.0012	0.0018	0.002	0.0042
C [μF]	22.35	24.65	33.30	22.03	19.54	9.45
R [Ω]	59.63	59.82	59.87	59.82	60.21	56.86
CPU time [s]	47.06	44.46	44.89	50.15	52.10	50.90
$J_{1\text{-}LCL}$ *final value*	**0.603**	**0.558**	**0.612**	**0.578**	**0.596**	**0.569**

solution results in specific filter resonant frequency; required amount of total inductance and specific THD of grid current. Such flexibility achieved by evolutionary search optimization helps the system designer to choose the most convenient filter parameters to apply. All PSO-based solutions satisfy the design criteria.

The evolution of objective function $J_{1\text{-}LCL}$ for the group of solutions of Table 6 are plotted and illustrated in Fig. 6. The obtained results indicate that the PSO algorithm converges to the final value and leads to a group of solution that are approximately similar for both cases of initial solutions.

Thus, the PSO can run at any arbitrary random initial solutions unlike many other algorithms that would trap in local minimum errors unless the initial solution are carefully selected. The bode diagram of filter transfer functions $Y_{21\text{-}LCL}$ and $h_{21\text{-}LCL}$ are plotted in Figs. 7 and 8 for zero initial solution # 1 and unity initial solutions # 2. For both group of solutions, the transfer function $Y_{21\text{-}LCL}$ have approximately similar attenuation for all frequency

Table 6
Some extreme optimum solutions of (L-RC-L) filter obtained from PSO.

Solution / Parameter	Zero initial solution		Unity initial solution	
	1	**2**	**1**	**2**
L_1 [H]	0.0030	7.1637e-04	8.8623e-04	0.0040
L_2 [H]	0.0019	4.5101e-04	7.5324e-04	0.0013
C [μF]	8.6	5.71	3.8877	10
R [Ω]	59.98	59.29	59.81	59.6
CPU Time [sec]	50.1	66.7	57.8	50.7
Resonant frequency [kHz]	**1.59**	**4**	**4**	**1.60**
THD of grid current [%]	**4.82**	**8.85**	**5.54**	**4.31**
Total inductance (L_1+L_2) [H]	**0.0049**	**0.0012**	**0.0016**	**0.0053**

range from 10 Hz up to 1000 kHz of −20 db/decade. Also, for high frequency range, the attenuation rate is the same of −40 db/decade. While, there is a slight difference in phase shift above 1 kHz. For transfer function $h_{21\text{-LCL}}$ both group of solutions lead to similar attenuation rate up to frequency of 3 kHz. In general, both group of solutions lead to similar characteristics (magnitude and phase shift) at low frequency range which is the main purpose to insert the filter between inverter and grid. In general, both group of solutions result in similar filter response at grid frequency of either 50 Hz or even 60 Hz. So, any group of solution can be utilized to realize the filter.

The obtained group of solutions of grid filter are plugged into the H/W model of the overall system to assess the performance. The resultant waveforms of grid currents at unity PF operation and the corresponding harmonic spectra are plotted in Figs. 9 and 10 respectively. The obtained results prove that both group of solutions obtained from the PSO algorithm are valid and applicable. Accordingly, the evolutionary PSO search method is successful to optimize the customized objective function $J_{1\text{-LCL}}$ to find suitable values of the passive components of grid filter.

The THD of the current injected to the grid in case of group of solution of (zero initial solution # 1) is 0.0482 (4.82%). While in case of (unity initial solution # 2) the THD of grid current is 0.0431 (4.31%) as well, where both of them match and satisfy the IEEE519 standard (Jayalath and Hanif, 2018; IEEE Recommended Practice, 2014).

6.2. Case 2: LLCL trap filter

6.2.1. Formulation of multi-objective function

The circuit diagram of trap filter is illustrated in Fig. 3e, whose passive components L_1, L_2, L_t and C_t to be determined. The corresponding transfer functions of Trap Filter given in Table 1 is presented again in Eqs. (14.1) and (14.2).

$$Y_{21\text{-trap}} = \frac{I_2(s)}{V_{conv}(s)} = \frac{\left(S^2 C_t L_t + 1\right)}{S^3 C_t (L_1 L_2 + L_2 L_t + L_1 L_t) + S(L_2 + L_1)} \tag{14.1}$$

$$h_{21\text{-trap}} = \frac{I_2(s)}{I_1(s)} = \frac{\left(S^2 C_t L_t + 1\right)}{S^2 C_t (L_2 + L_t) + 1} \tag{14.2}$$

The objective function J_{2-trap} is elaborated to include three terms: harmonic attenuation, size of inductors L_1, L_2, L_t and size of Capacitor C_t.

$$J_{2-trap} = min\left[Y_{21\_trap} + \left(\frac{L_1 + L_2}{L_B} + \frac{C}{C_B}\right)\right] \tag{15}$$

6.2.2. PSO obtained results

Some optimum solutions of trap filter obtained from the PSO algorithm are presented in Table 7. Each PSO group of solution results in specific filter resonant frequency; trap frequency; required amount of total filter inductance and specific THD of grid current. Both filter resonant frequency and trap frequency satisfy the design criteria. Accordingly, system designer has flexibility to choose the most convenient solution to be realized to achieve minimum cost or to satisfy minimum THD of grid current. The evolution of objective function J_{2_trap} for the group of solutions of Table 7 are presented in Fig. 11. The obtained results indicate that the PSO algorithm converges to approximately similar final values irrespective the initial guess values. However, with zero initial solution the PSO algorithm took fewer iterations (18 iterations) to reach to the final value. While in the case of unity initial solution, the PSO algorithm converged to the final value after longer number of iterations (36 iteration).

The bode diagram of the transfer function $Y_{21\text{-trap}}$ is sketched in Fig. 12. In Fig. 12a, the bode diagram has been plotted for the zero initial solution # 1 of Table 7 (L_1 = 1.4 mH, L_2 = 1.4 mH, L_t = 1 mH, C_t = 17.9 μF). The resultant resonant frequency is 0.912 kHz and the resultant trap frequency is 1.18 kHz that satisfy the filter design restrictions.

While in Fig. 12b, the bode diagram has been sketched for the unity initial solution # 1 of Table 7 (L_1 = 1.2 mH, L_2 = 1.3 mH, L_t = 0.11 mH, C_t = 2.3 μF). The resultant resonant frequency and trap frequency are 4 kHz and 10 kHz respectively, which are in accordance with the filter design restrictions.

According to the results, trap filter provides strong attenuation at the trap frequency f_{trap} (Fang et al., 2017a). In addition, the trap filter maintains relatively high attenuation at high frequency range. However, there is a resonant peak at resonant frequency f_{res} that is practically attenuated by adding a small resistor in series with the trap branch (L_t C_t) (Li et al., 2015).

The waveform of grid current at unity PF is plotted in Fig. 13 for both selected solutions. The corresponding harmonic spectrum is illustrated in Fig. 14. As presented in Table 7 the THD of the current injected to the grid is 0.0329 (3.29%) with the zero initial solution # 1, and the THD of the current is 0.0282 (2.82%) for unity initial solution # 1, such values are in a complete accordance with the IEEE-519 standard (Jayalath and Hanif, 2018; IEEE Recommended Practice, 2014).

6.3. Assessment of PSO obtained results

In order to determine to what degree the evolutionary search approach based on PSO technique is effective and successful

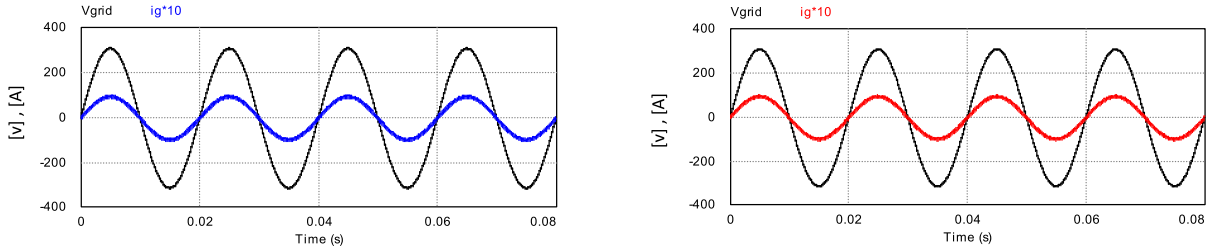

Fig. 9. Steady state waveforms of grid current and voltage at unity PF with (L-RC-L) filter for both groups of solutions.

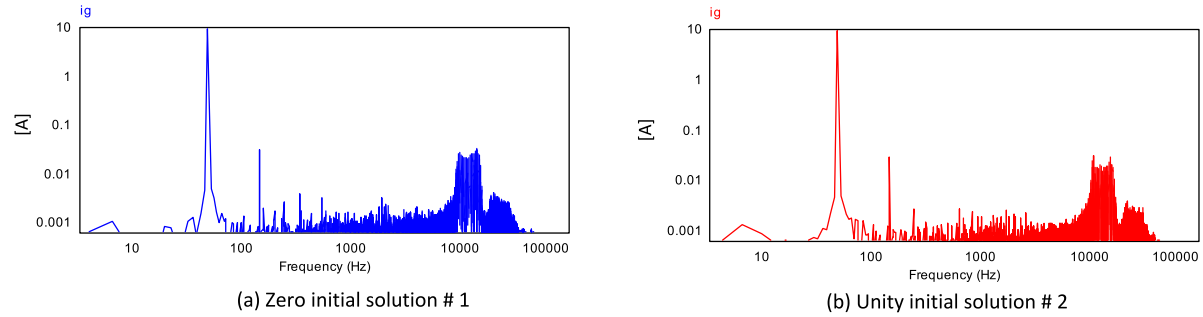

Fig. 10. Harmonic spectrum of grid current with (L-RC-L) filter for both groups of solutions.

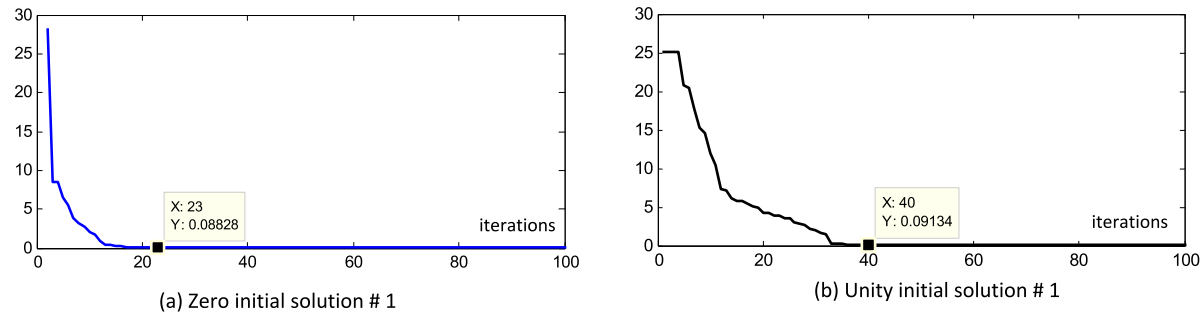

Fig. 11. Evolution of objective function J_{2_trap}.

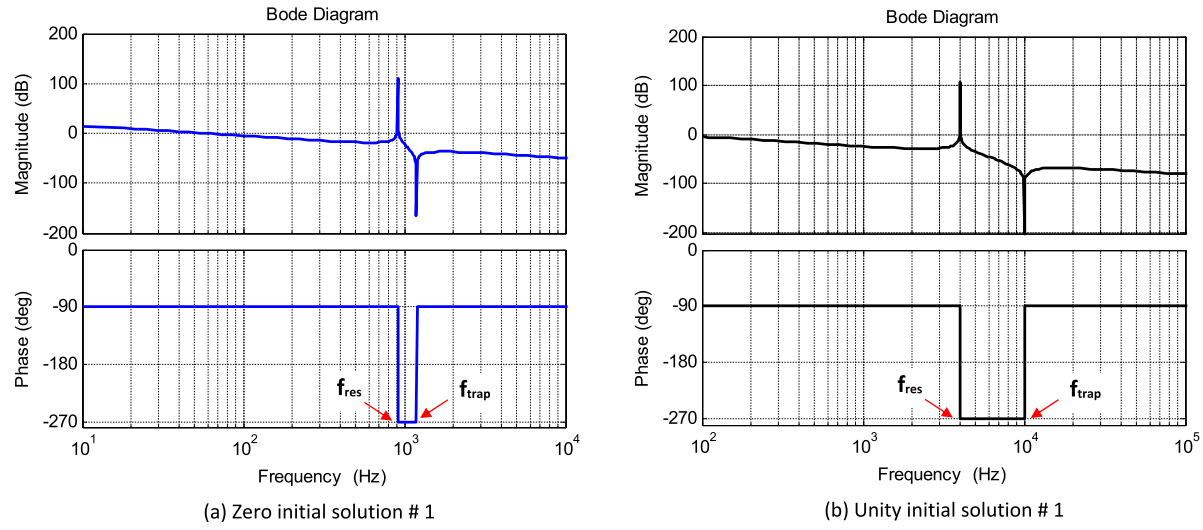

Fig. 12. Bode diagram of filter transfer function $Y_{21\text{-}trap}$ of trap filter.

Table 7
Some optimum solutions of trap filter obtained from PSO.

Parameter \ Solution	Zero initial solution		Unity initial solution	
	1	**2**	**1**	**2**
L_1 [H]	0.0014	0.0011	0.0012	0.0021
L_2 [H]	0.0014	0.0012	0.0013	0.0022
L_t [H]	0.0010	1.1e-4	1.19e-4	2.03e-04
C_t [μF]	17.9	2.3	2.12	1.24
Resonant Frequency [kHz]	**0.912**	**4**	**4**	**4**
Trap Frequency [kHz]	**1.18**	**10**	**10**	**10**
THD of grid current [%]	**3.09**	**3.29**	**2.82**	**1.62**
Total inductance (L_1+L_2+L_t) [H]	**0.0038**	**0.0023**	**0.0026**	**0.0045**

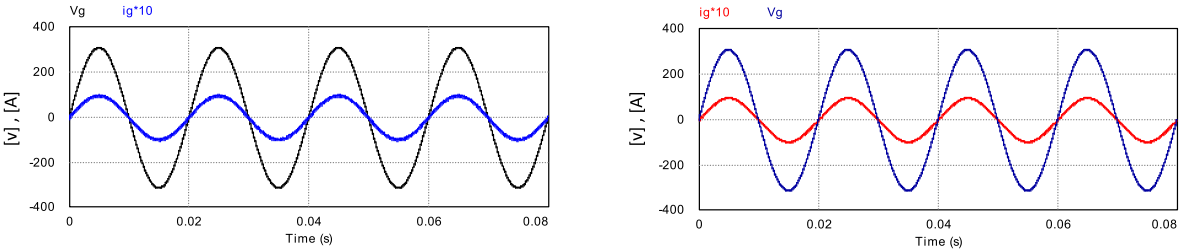

(a) Zero initial solution # 1 (b) Unity initial solution # 1

Fig. 13. Steady state waveforms of grid current and voltage with trap filter at unity PF.

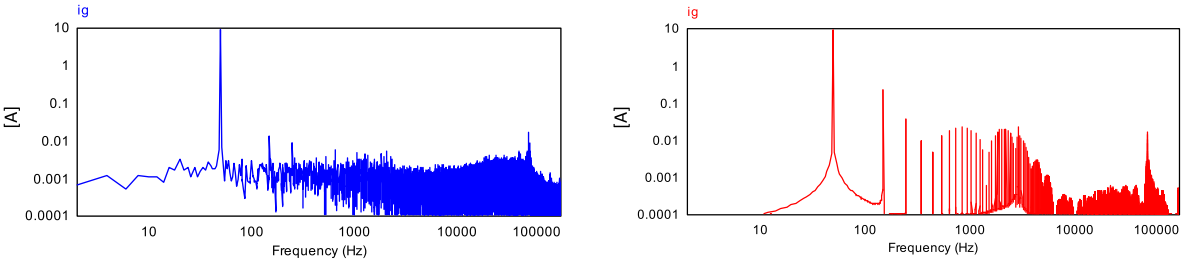

(a) Zero initial solution # 1 (b) Unity initial solution # 1

Fig. 14. Harmonic spectrum of grid current with trap filter for both groups of solutions.

to determine the optimum values of high order passive filters elements, the harmonic spectra of ac current injected to the grid have been plotted for arbitrary chosen obtained solutions of both filter schemes studied in this article. The corresponding harmonic spectra are compared with the maximum allowable limits mentioned in IEEE 519 standard as illustrated in Fig. 15.

Fig. 15a illustrates the harmonic spectrum of the current injected to the grid in case of LCL filter with the group of solution ($L_1 = 3$ mH, $L_2 = 1.9$ mH, $C = 8.6$ μF, $R = 59.98$ Ω). Owing to the results, the optimum values of the LCL filter achieved by PSO algorithm satisfy the grid code restrictions and harmonics limitations given by IEEE 519 standard.

Moreover, the optimum values of trap filter elements determined by the PSO technique satisfy also the IEEE 519 standard as shown in Fig. 15b for the group of solution ($L_1 = 1.4$ mH, $L_2 = 1.4$ mH, $L_t = 1$ mH, $C_t = 17.9$ μF). The results indicate that, trap filter provides relatively better harmonic attenuation and lower THD compared with LCL filter (IEEE Recommended Practice, 2014).

7. Comparison with conventional design approach

A comparison between passive grid filter design using conventional method and multi-objective evolutionary search approach has been addressed in this section for both types of grid filter investigated in this article: LCL filter and Trap filter for the system whose rating and base values are given in Table 2. The inverter output voltage waveform is assumed to be bipolar (Ruan et al., 2018).

Both methodologies have been compared in terms of extreme (maximum/minimum) computed values of filter passive elements (individual inductors and capacitors) and the total inductance required to realize the filter.

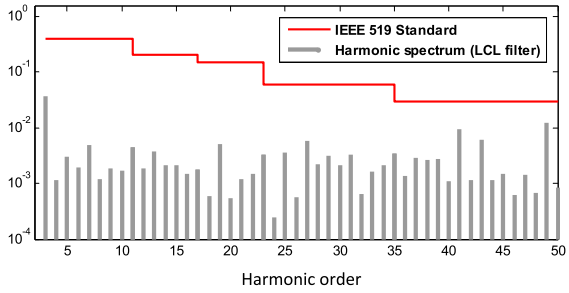

Fig. 15a. Harmonic spectrum of grid current with LCL filter ($L_1 = 3$ mH, $L_2 = 1.9$ mH, $C = 8.6$ μF, $R = 59.98$ Ω).

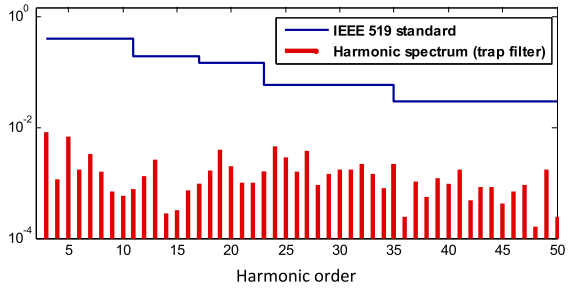

Fig. 15b. Harmonic spectrum of grid current with trap filter ($L_1 = 1.4$ mH, $L_2 = 1.4$ mH, $L_t = 1$ mH, $C_t = 17.9$ μF).

Conventional design method of passive grid filter discussed before in Section 4.1 is summarized in Tables (Table 8a and Table 9a) for LCL and Trap filters respectively. The conventional design procedure is based on four major constrains: maximum allowable reactive power, maximum allowable total inductance, range of inverter-side ripple current and resonant frequency constrain. A fifth constrain (filter trap frequency) is added in the case of trap filter.

(a) The maximum allowable capacitive reactive power (Q_c) through filter capacitor should not exceed 5% of the rated active power (Jayalath and Hanif, 2018; Anzalchi et al., 2017).
(b) The upper limit of overall total inductance should be between (10%–25%) of the base value (0.1–0.25 pu) in order to limit the voltage drop across the filter inductors (Rockhill and others, 2011). So, restricting the upper allowable limit of the total inductance to 20% of the base value is accepted.
(c) The inverter-side ripple current should be less than 40% of rated reference peak current (Xu et al., 2014; Anzalchi et al., 2016). So, an upper and lower limits bounded to (15%–20%) of the peak value of the rated current injected to the grid should result in satisfactory current waveform (Anzalchi et al., 2016, 2017; Chayjani and Monfared, 2016).
(d) The filter resonant frequency should satisfy the range determined by the relation ($10\, f_g < f_{res} < 0.5\, f_{swt}$) to avoid resonance inside the control bandwidth (Jayalath and Hanif, 2018; Wu et al., 2012; Romdhane et al., 2017).
(e) In case of trap filter, the trap frequency is chosen to be the same as the maximum switching frequency of the inverter ($f_{trap} = f_{swt}$) (Wu et al., 2012).

Accordingly, the computed numerical results are presented in Tables 8b and 9b for LCL and Trap filters respectively.

7.1. LCL filter

See Table 8a.

Table 8a
Summary of conventional design methodology of LCL filter.

Constrain	Mathematical formula	Parameter
Reactive power constrain	$Q_{cmax} = 0.05P_{rated}$	C_{max} $C < C_{max}$
Total inductance constrain	$L_{total-max} = 0.2L_B$ $L_{total-max} = (L_1 + L_2)$	$L_{total-max}$
Inverter-side ripple current	$\Delta I_{L1} = \frac{V_{DC}}{2L_1 f_{swt}}$ $I_{min} < \Delta I_{L1} < I_{max}$ $I_{min} = 0.15I_{rated-peak}$ $I_{max} = 0.20I_{rated-peak}$	L_{1min}; L_{1max} L_{2min}; L_{2max}
Resonant frequency constrain	$10f_g < f_{res} < 0.5f_{swt}$ $f_{swt(max)} = 10$ kHz	*Checking* L_1; L_2
Filter resonant frequency	$f_{res} = \frac{1}{2\pi}\sqrt{\frac{(L_1 + L_2)}{L_1 L_2 C}}$	

Table 8b
Comparison between conventional design method and PSO approach for LCL filter.

Filter Parameter	Conventional Design	Evolutionary Search Approach
C_{max}	13.15 μF	10 μF
$L_{total-max}$	7.70 mH	5.3 mH
L_1	(3.89 - 5.19) mH	(0.71 – 4.0) mH
L_2	(2.51 - 3.81) mH	(0.45 – 1.9) mH
L_1+ L_2	(6.4 - 9.0) mH	(1.16 – 5.9) mH

Compared with conventional design methodology, the LCL grid filter design based on multi-objective evolutionary search

Table 9a
Summary of conventional design methodology of LLCL trap filter.

Constrain	Mathematical formula	Parameter
Reactive power constrain	$Q_{cmax} = 0.05P_{rated}$	C_{tmax} $C_t < C_{tmax}$
Filter trap frequency	$f_{trap} = \frac{1}{2\pi\sqrt{L_t C_{tmax}}}$	L_{tmin}
Total inductance constrain	$L_{total-max} = 0.2L_B$ $L_{total-max} = (L_1 + L_2)$	$L_{total-max}$
Inverter-side ripple current	$\Delta I_{L1} = \frac{V_{DC}}{2L_1 f_{swt}}$ $I_{min} < \Delta I_{L1} < I_{max}$ $I_{min} = 0.15I_{rated-peak}$ $I_{max} = 0.20I_{rated-peak}$	L_{1min}; L_{1max} L_{2min}; L_{2max}
Resonant frequency constrain	$10f_g < f_{res} < 0.5f_{swt}$ $f_{swt(max)} = 10$ kHz	*Checking* $L_1; L_2$
Filter resonant frequency	$f_{res} = \frac{1}{2\pi}\sqrt{\frac{(L_1 + L_2)}{C_t\,(L_1L_2 + L_2L_t + L_tL_1)}}$	

Table 9b
Comparison between conventional design method and PSO approach for trap filter.

Filter Parameter	Conventional Design	Evolutionary Search Approach
$C_{t\,max}$	13.15 μF	17.9 μF
C_t	$C_t < C_{t\,max}$ ($C_t = 0.5\ C_{t\,max}$) = 5.45 μF	2.12 μF
$L_{t\,min}$	0.046 mH	0.11 mH
L_t	0.1 mH	0.11 mH
$L_{total\text{-}max}$	7.7 mH	4.3 mH
L_1	(3.89 – 5.19) mH	(1.1 – 2.1) mH
L_2	(2.51 - 3.81) mH	(1.2 – 2.2) mH
$L_1 + L_2$	(6.40 - 9.00) mH	(2.3 – 4.3) mH

approach provides lower numerical values of passive components needed to realize the filter as shown in the tabulated results of Table 8b. In addition, other parameters would be involved in the customized objective function to achieve other goals upon the request of system designer, which is not possible in conventional design approach.

7.2. Trap filter

See Table 9a.

According to the results of comparison, the trap filter design based on multi-objective evolutionary search approach provides lower numerical values of individual inductors and total inductance.

It is observed that one obtained solution from PSO algorithm results in a maximum capacitor (C_{tmax}) of 17.9 μF (which is higher than the value 13.15 μF obtained from conventional approach). However, in many obtained solutions by PSO algorithm, lower numerical values for the capacitor C_t are obtained and can be chosen for filter realization as indicated by the results of Table 9b (the chosen value for the capacitor is $C_t = 2.12$ μF).

Moreover, other design parameters can be involved in the customized objective function such that the optimum design can take into consideration other goals, which is not possible in conventional design procedure.

8. Conclusion

This article presents a non-traditional design approach of high order passive grid filter for single-phase grid integration system using particle swarm optimization as a multi-objective evolutionary search technique.

The design approach aims to find the optimum numerical values of the passive filter that optimize simultaneously multiple factors: harmonic attenuation and the size of filter components (inductors and capacitors).

The study has been conducted on two different schemes of high order passive filters (LCL with damping resistor, and trap filter). The optimum values of passive filters obtained from the PSO algorithm have been plugged into a single-phase grid integration model elaborated in PSIM® simulation package.

Owing to the obtained results, the multi-objective evolutionary search approach is effective to provide an optimum design of passive grid filter that satisfies the existing codes of grid integration such as IEEE standard 519.

The main contribution of this paper is the utilization of evolutionary optimization technique to achieve an optimum design of passive grid filter, where the multi-objective design approach provides successfully non-unique solution to the optimization problem. Thus, the system designer can select (among several obtained solutions) the most appropriate values of filter components from technical point of view (lowest THD and highest harmonic attenuation) or from economic point of view (lowest cost, lowest size and availability in market).

In addition, a comparison between conventional design approach and multi-objective evolutionary search design approach has been carried out. The obtained results indicate that filter design based on multi-objective evolutionary search approach results in lower numerical values of the passive elements of grid filter, which achieves considerable reduction in the size and cost of the passive grid filter. Moreover, evolutionary search approach permits accommodation of several design criteria in the customized objective function with arbitrary weighting factors owing to design priorities or requirements and restrictions of possible new grid codes.

Declaration of competing interest

The authors declare that they have no known competing financial interests or personal relationships that could have appeared to influence the work reported in this paper.

Appendix

A.1. Generalized form of grid filter transfer functions

The generalized form of passive grid filter transfer functions (I_2/V_{conv}) and (I_2/I_1) have been derived by dealing with the passive grid filter as Two-Port Network and determining *Y*-model p and *h*-model Parameters.

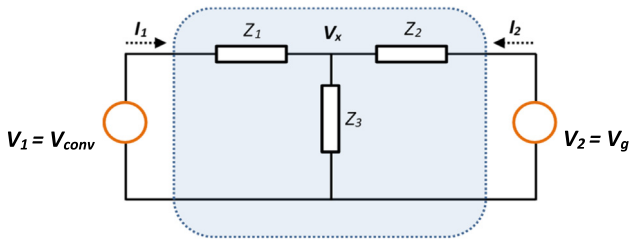

Fig. A.1. Generalized scheme of passive grid filter.

A.1.1. General form of transfer function $I_2(s)/V_{conv}(s)$

Owing to the generalized circuit diagram of passive grid filter shown in Fig. A.1, the *Y*-parameters model described by Eqs. (A.1) and (A.2) can be determined.

$$I_1 = Y_{11}V_1 + Y_{12}V_2 \tag{A.1}$$

$$I_2 = Y_{21}V_1 + Y_{22}V_2 \tag{A.2}$$

where $Y_{21} = \frac{I_2}{V_1}\big|_{V_2=0}$; which represents the required transfer function of grid side current to the inverter output voltage. By applying KCL at node x:

$$\frac{V_1 - V_x}{Z_1} = \frac{V_x}{Z_3} + \frac{V_x}{Z_2} \Rightarrow V_x = V_1\frac{Z_2Z_3}{Z_1Z_2 + Z_2Z_3 + Z_1Z_3} \tag{A.3}$$

$$i_2 = \frac{V_x}{Z_2} \Longrightarrow i_2 = V_1\frac{Z_2Z_3/Z_2}{Z_1Z_2 + Z_2Z_3 + Z_1Z_3} \tag{A.4}$$

Therefore, the transfer function $I_2(s)/V_{conv}(s)$ is obtained:

$$Y_{21} = \frac{I_2(s)}{V_{conv}(s)} = \frac{Z_3}{Z_1Z_2 + Z_2Z_3 + Z_1Z_3} \tag{A.5}$$

A.1.2. General form of transfer function $I_2(s)/I_1(s)$

The transfer function (I_2/I_1) is also deduced with the aid of *h*-parameters model of the two-port network shown in Fig. A.1. The *h*-parameter model is described by Eqs. (A.6) and (A.7):

$$V_1 = h_{11}I_1 + h_{12}V_2 \tag{A.6}$$

$$I_2 = h_{21}I_1 + Y_{22}V_2 \tag{A.7}$$

where $h_{21} = \frac{I_2}{I_1}\big|_{V_2=0}$; which represents the transfer function of grid side current to the inverter output current. i.e. h_{21} is the ratio between output and input current of the passive filter. Owing to Fig. 8.1, the filter output current i_2 is determined by Eq. (A.8) which is a replica of Eq. (A.4) previously deduced in part 1.

$$i_2 = \frac{Z_3V_1}{Z_1Z_2 + Z_2Z_3 + Z_1Z_3} \tag{A.8}$$

The filter input current i_1 is also derived : $i_1 = \frac{V_1 - V_x}{Z_1}$ (A.9)

$$i_1 = \frac{V_1 - V_1\frac{Z_2Z_3}{Z_1Z_2+Z_2Z_3+Z_1Z_3}}{Z_1} \tag{A.10}$$

$$i_1 = \frac{\left(1 - \frac{Z_2Z_3}{Z_1Z_2+Z_2Z_3+Z_1Z_3}\right)V_1}{Z_1}; \tag{A.11}$$

$$i_1 = \frac{V_1}{Z_1}\frac{Z_1Z_2 + Z_1Z_3}{Z_1Z_2 + Z_2Z_3 + Z_1Z_3} \tag{A.12}$$

Thus, the transfer function $I_2(s)/I_1(s)$ is obtained:

$$h_{21} = \frac{I_2(s)}{I_1(s)} = \frac{Z_1Z_3}{Z_1Z_2 + Z_1Z_3}; \tag{a.13.1}$$

$$h_{21} = \frac{I_2(s)}{I_1(s)} = \frac{Z_3}{Z_2 + Z_3} \tag{a.13.2}$$

A.2. Transfer functions of L-RC-L filter

A.2.1. Transfer function $I_2(s)/V_{conv}(s)$

In case of LCL-filter with damping resistor R, the impedances $Z_1 = SL_1$, $Z_2 = SL_2$ and $Z_3 = \left(R + \frac{1}{SC}\right)$. Accordingly, the transfer function Y_{21} is to be:

$$Y_{21\text{-LCL}} = \frac{\left(R + \frac{1}{SC}\right)}{SL_1SL_2 + SL_2\left(R + \frac{1}{SC}\right) + SL_1\left(R + \frac{1}{SC}\right)} \tag{A.14}$$

$$Y_{21\text{-LCL}} = \frac{I_2(s)}{V_{conv}(s)} = \frac{\left(R + \frac{1}{SC}\right)}{S^2L_1L_2 + SR\left(L_2 + L_1\right) + \frac{1}{C}\left(L_2 + L_1\right)} \tag{A.15}$$

$$\therefore \frac{I_2\,(s)}{V_{conv}\,(s)} = \frac{\frac{1}{L_1L_2}\left(R + \frac{1}{SC}\right)}{S^2 + SR\left(\frac{L_2+L_1}{L_1L_2}\right) + \frac{1}{C}\left(\frac{L_2+L_1}{L_1L_2}\right)} \tag{A.16}$$

By comparing the denominator characteristics equation of Eq. (A.16) with the standard 2nd order form $\left(S^2 + 2\xi\omega_{r1}S + \omega_{r1}^2\right)$ both resonant radian frequency ω_{r1} (Xu et al., 2013; Li et al., 2018b) and filter damping factor ξ_1 are determined and formulated in Eqs. (A.17) and (A.18):

$$\omega_{r1}^2 = \left(\frac{L_2 + L_1}{L_1L_2C}\right) \Rightarrow \omega_{r1} = \sqrt{\left(\frac{L_2 + L_1}{L_1L_2C}\right)} \tag{A.17}$$

$$2\xi_1\,\omega_n = R\left(\frac{L_2 + L_1}{L_1L_2}\right) \Rightarrow \xi_1 = \frac{R}{2}\sqrt{C\left(\frac{L_2 + L_1}{L_1L_2}\right)} \tag{A.18}$$

A.2.2. Transfer function $I_2(s)/I_1(s)$

By substituting the impedances Z_1, Z_2 and Z_3 with their corresponding values of LCL-filter, the transfer function h_{21} is obtained and formulated in Eqs. (A.19)–(A.21):

$$h_{21\text{-LCL}} = \frac{I_2(s)}{I_1(s)} = \frac{SL_1\left(R + \frac{1}{SC}\right)}{SL_1SL_2 + SL_1\left(R + \frac{1}{SC}\right)} \tag{A.19}$$

$$\frac{I_2(s)}{I_1(s)} = \frac{SL_1\left(R + \frac{1}{SC}\right)}{SL_1SL_2 + SL_1\left(R + \frac{1}{SC}\right)} = \frac{\left(R + \frac{1}{SC}\right)}{SL_2 + \left(R + \frac{1}{SC}\right)} \tag{A.20}$$

$$\therefore \frac{I_2(s)}{I_1(s)} = \frac{SCR + 1}{S^2L_2C + SCR + 1} = \frac{\frac{1}{L_2C}\left(SCR + 1\right)}{\left(S^2 + S\frac{R}{L_2} + \frac{1}{L_2C}\right)} \tag{A.21}$$

Similarly, as carried out in the previous section, by comparing the denominator characteristics equation of Eq. (A.21) with the standard 2nd order form $\left(S^2 + 2\xi\omega_{r2}S + \omega_{r2}^2\right)$ both resonant radian frequency ω_{r2} and filter damping factor ξ_2 are determined and formulated in Eqs. (A.22) and (A.24):

$$\omega_{r2}^2 = \left(\frac{1}{L_2C}\right) \Rightarrow \omega_{r2} = \sqrt{\frac{1}{L_2C}} \tag{A.22}$$

$$2\xi_2\,\omega_{r2} = \left(\frac{R}{L_2}\right) \Rightarrow \xi_2 = \frac{R}{2L_2}\sqrt{L_2C} \tag{A.23}$$

$$\xi_2 = \frac{R}{2}\sqrt{\frac{C}{L_2}} \tag{A.24}$$

A.3. Items' specifications and simulation parameters

See Table A.1.

Table A.1
Specifications of the investigated system.

Parameter	Value
Inverter power device	
Type	IGBT branch module
Device number & Rating	SKM75GB12T4 , 1200 V–75 A
AC bus	$1-\Phi$
Line–line voltage	220 V/50 Hz
DC bus	
Operating voltage	400 V
PV array	
Peak output power	5.12 kW @ STC
PV module model & Rating	SUNPOWER E19/320 (320 W)
Number of modules	16 (4 series × 4 parallel paths)
PEM-FC	
Maximum output power	4.8 kW
Single FC stack	Nexa 1200 (1200 W)
DC voltage (single stack)	20–36 V
Number of FC units	4 (connected in series)
Battery Bank	
Type	Deep cycle gel battery
Total capacity	100 Ah
Single battery	Power sonic 12 V/100 Ah
Number of batteries	10 (connected in series)
Total DC voltage	120 V
Passive grid filters	
LCL with R	PSO-based results of Table 6
Trap filter	PSO-based results of Table 7
Simulation platforms	
H/W circuits simulation	PSIM® professional version 9.0.3
PSO algorithm	Matlab R2014a
Simulation step time	
PSIM package	10 μs

A.4. Nomenclatures

Y_{21}: Admittance of Y-parameter model of two-port network
h_{21}: Short circuit current gain of *h*-parameter model of two-port network
$Y_{21\text{-}LCL}$: Admittance of Y-parameter model of LCL filter
$h_{21\text{-}LCL}$: Short circuit current gain of *h*-parameter model of LCL filter
$Y_{21\text{-}trap}$: Admittance of Y-parameter model of trap filter
$h_{21\text{-}trap}$: Short circuit current gain of *h*-parameter model of trap filter
V_{DC}: DC bus voltage
V_{PV}: PV array voltage
V_{FC}: Fuel Cell voltage
V_{BAT}: Voltage of battery bank
d_{pv}: Duty cycle of PV dc–dc converter
d_{fc}: Duty cycle of fuel cell dc–dc converter
d_{bat}: Duty cycle of battery bank dc–dc converter
Z_B: System base impedance
C_B: Base capacitance
L_B: Base inductance
L_1: Inverter side inductor
L_2: Grid side inductor
L_{total} Total inductance (L_1+L_2)
$L_{total-max}$ Maximum total inductance $(L_1+L_2)_{max}$
L_t: Inductor of series resonant branch of trap filter
$L_{t\ min}$: Minimum inductance of series resonant branch of trap filter
C_t: Capacitor of series resonant branch of trap filter
C_{tmax}: Maximum capacitance of series resonant branch
C: Capacitor of LCL filter
C_{max}: Maximum capacitance of LCL filter
Q_c: Capacitive reactive power
R: Damping resistor of LCL filter
$J_{1\text{-}LCL}$: Objective function of PSO algorithm for LCL filter
J_{2-trap}: Objective function of PSO algorithm for trap filter
f_{res}: Resonant frequency of trap filter
f_{trap}: Trap frequency of series resonant branch of the trap filter
f_{swt}: Inverter switching frequency
w: Inertia weight of PSO algorithm
$\alpha,\ \beta$ Uniformly distributed positive random vector of PSO algorithm
k: Iteration number k of the PSO algorithm
i: Particle number i of the PSO algorithm
G Global best position found by all particles
L Local (Particle) best position
v_i^k Velocity of the particle i at iteration k
ω_{r1} Resonant radian frequency of filter transfer function Y_{21} of LCL filter
ω_{r2} Resonant radian frequency of filter transfer function h_{21} of LCL filter

A.5. Abbreviations

ACO:	Ant Colony
BBO:	Biogeography-Based Optimization
DER:	Distributed Energy Resources
FC:	Fuel Cell
GA:	Genetic Algorithm
kWP:	Kilo Watt Peak
PEM:	Proton Exchange Membrane
PF:	Power Factor
PSO:	Particle Swarm Optimization
PV:	Photovoltaic
STC:	Standard Test Conditions
THD:	Total Harmonic Distortion
VSI:	Voltage Source Inverter

References

Aghajani, G., Ghadimi, N., 2018. Multi-objective energy management in a micro-grid. Energy Rep. 4, 218–225.

Al-Roomi, A.R., El-Hawary, M.E., 2019. Optimal coordination of double primary directional overcurrent relays using a new combinational BBO/DE algorithm. Can. J. Electr. Comput. Eng. 42 (3), 135–147.

Anzalchi, A., Moghaddami, M., Moghadasi, A., et al., 2016. A new topology of higher order power filter for single-phase grid-tied voltage-source inverters. IEEE Trans. Ind. Electron. 63 (12), 7511–7522.

Anzalchi, A., Moghaddami, M., Moghadasi, A., et al., 2017. Design and analysis of a higher order power filter for grid-connected renewable energy systems. IEEE Trans. Ind. Appl. 53 (5), 4149–4161.

Azab, M., 2015. Identification of one-diode model parameters of PV devices from nameplate information using particle swarm and least square methods. In: Proceedings of IEEE Smart Grid & Ren Energy SGRE'15.

Azab, Mohamed, 2017. Flexible PQ control for single-phase grid-tied photovoltaic inverter. In: IEEE Int. Conf. on Environment and Electrical Engineering (EEEIC / I & CPS Europe). http://dx.doi.org/10.1109/EEEIC.2017.7977550.

Azab, M., 2018. Intra-minutes technical impacts of PV grid integration on distribution network operation of a rural community under extreme PV power delivery. In: Journal of Energy Systems. Springer-Verlag, Germany, http://dx.doi.org/10.1007/s12667-018-0307-7.

Azab, M., 2019. Performance of model predictive control approach for single-phase distributed energy grid integration with PQ control. IET Energy Syst. Integr. http://dx.doi.org/10.1049/iet-esi.2018.0031.

Beres, R.N., 2016. A review of passive power filters for three-phase grid-connected voltage-source converters. IEEE J. Emerg. Sel. Top. Power Electron. 4 (1), 54–69.

Chayjani, M.S., Monfared, M., 2016. Design of LCL and LLCL filters for single-phase grid connected converters. IET Power Electron. 9 (9), 1971–1978.

Chayjani, M.S., Monfared, M., 2016b. Stability analysis and robust design of LCL with multituned traps filter for grid-connected converters. IEEE Trans. Ind. Electron. 63 (11), 6823–6834.

Chayjani, M.S., Monfared, M., 2018. High-order filter design for high-power voltage-source converters. IEEE Trans. Ind. Electron. 65 (1), 49–58.

Corus, D., Oliveto, P.S., 2018. Standard steady state genetic algorithms Can hill climb faster than mutation-only evolutionary algorithms. IEEE Trans. Evol. Comput. 22 (5), 720–732.

Fang, J., Li, H., Tang, Y., 2017a. A magnetic integrated LLCL filter for grid-connected voltage-source converters. IEEE Trans. Power Electron. 32 (3), 1725–1730.

Fang, J., Li, X., Yang, X., et al., 2017b. An integrated trap-LCL filter with reduced current harmonics for grid-connected converters under weak grid conditions. IEEE Trans. Power Electron. 32 (11), 8446–8457.

Fang, J., Xiao, G., Yang, X., et al., 2017c. Parameter design of a novel series-parallel-resonant LCL filter for single-phase half-bridge active power filters. IEEE Trans. Power Electron. 32 (1), 200–217.

Han, C., Wang, L., Zhang, Z., et al., 2018. Multi-objective genetic algorithm based on fitting and interpolation. IEEE Access 6, 22920–22929.

2014. IEEE recommended practice and requirements for harmonic control in electric power systems, IEEE std. 519-2014. pp. 1–29, (Revision of IEEE Std 519-1992).

Jayalath, S., Hanif, M., 2018. An LCL-filter design with optimum total inductance and capacitance. IEEE Trans. Power Electron. 33 (8), 6687–6698.

Leboucher, C., Shin, H.S., Chelouah, R., et al., 2018. An enhanced particle swarm optimization method integrated with evolutionary game theory. IEEE Trans. Games 10 (2), 221–230.

Lee, H.J., Song, J.Y., Kim, D.W., et al., 2018. Particle swarm optimization algorithm with intelligent particle number control for optimal design of electric machines. IEEE Trans. Ind. Electron. 65 (2), 1791–1798.

Li, X., Fang, J., Lin, P., et al., 2018a. Active magnetic decoupling for improving the performance of integrated LCL-filters in grid-connected converters. IEEE Ind. Electron. 65 (2), 1367–1376.

Li, X., Fang, J., Tang, Y., et al., 2018b. Capacitor-voltage feedforward with full delay compensation to improve weak grids adaptability of LCL-filtered grid-connected converters for distributed generation systems. IEEE Trans. Power Electron. 33 (1), 749–764.

Li, F., Zhang, X., Zhu, H., et al., 2015. An LCL-LC filter for grid-connected converter: Topology, parameter, and analysis. IEEE Trans. Power Electron. 30 (9), 5067–5077.

Liu, W., Wang, Z., Lui, X., et al., 2019. A novel particle swarm optimization approach for patient clustering from emergency departments. IEEE Trans. Evol. Comput. 23 (4), 632–644.

Liu, Z.H., Wei, H.L., Zhong, Q.C., et al., 2017. Parameter estimation for VSI-Fed PMSM based on a dynamic PSO with learning strategies. IEEE Trans. Power Electron. 32 (4), 3154–3165.

Liu, X.F., Zhan, Z.H., Deng, J.D., et al., 2018. An energy efficient ant colony system for virtual machine placement in cloud computing. IEEE Trans. Evol. Comput. 22 (1), 113–128.

Ma, Y.N., Gong, Y.J., Xiao, C.F., et al., 2019. Path planning for autonomous underwater vehicles: An ant colony algorithm incorporating alarm pheromone. IEEE Trans. Veh. Technol. 68 (1), 141–154.

Ma, H., Simon, D., Siarry, P., et al., 2017. Biogeography-based optimization: A 10-year review. IEEE Trans. Emerg. Top. Comput. Intell. 1 (5), 391–407.

Mahamat, C., Petit, N., Costa, F., et al., 2017. Optimized design of an LCL filter for grid connected photovoltaic system and analysis of the impact of neighbors' consumption on the system. J. Electr. Syst. 13 (4), 618–632.

Mohammadi, A., Asad, H., Mohamed, S., et al., 2019. Multiobjective and interactive genetic algorithms for weight tuning of a model predictive control-based motion cueing algorithm. IEEE Trans. Cybern. 49 (9), 3471–3481.

Ning, Y., Dai, Y., Peng, Z., 2019. GA–PSO approach for optimizing space-vector PWM control sequence. IET Power Electron. 12 (4), 955–965.

Radosavljevic, J., 2018. Overview of Particle Swarm Optimization. IET, http://dx.doi.org/10.1049/PBPO131E_ch3.

Rockhill, A., et al., 2011. Grid-filter design for a multimegawatt medium-voltage voltage-source inverter. IEEE Trans. Ind. Electron. 58 (4), 1205–1217.

Romdhane, M.B.S., et al., 2017. An improved LCL filter design in order to ensure stability without damping and despit large grid impedance variation. Energies 10 (336), http://dx.doi.org/10.3390/en10030336, MDPI.

Ruan, X., Wang, X., Pan, D., Yang, D., Li, W., Bao, C., 2018. Design of LCL filter. In: Control Techniques for LCL-Type Grid-Connected Inverters. In: CPSS Power Electronics Series, Springer, Singapore.

Sarker, K., Chatterjee, D., Goswami, S.K., 2018. Modified harmonic minimisation technique for doubly fed induction generators with solar-wind hybrid system using biogeography-based optimization. IET Power Electron. http://dx.doi.org/10.1049/iet-pel.2017.0818.

Sebtahmadi, S.S., Azad, H.B., Kaboli, A., et al., 2018. A PSO-DQ current control scheme for performance enhancement of z-source matrix converter to drive IM fed by abnormal voltage. IEEE Trans. Power Electron. 33 (2), 1666–1681.

Sharma, R., Goel, S., 2017. Performance analysis of a 11.2 kWp roof top grid-connected PV system in eastern India. Energy Rep. 3, 76–84.

Singh, S., Singh, B., 2014. Optimized passive filter design using modified particle swarm optimization algorithm for a 12-pulse converter-fed LCI–synchronous motor drive. IEEE Trans. Ind. Appl. 50 (4), 2681–2689.

Tan, Y., 2018. Swarm Intelligence Volume 3: Applications. IET, ISBN: 978-1-78561-631-0.

Tegou, T.I., Tsiflikiotis, A., Vergados, D.D., et al., 2018. Spectrum allocation in cognitive radio networks using chaotic biogeography-based optimisation. IET Netw. http://dx.doi.org/10.1049/iet-net.2017.0264.

Wang, Z., Li, J., Fan, K., et al., 2018a. Prediction method for low speed characteristics of compressor based on modified similarity theory with genetic algorithm. IEEE Access 6, 36834–36839.

Wang, X., Wang, G., Wu, Y., 2018b. An adaptive particle swarm optimization for underwater target tracking in forward looking sonar image sequences. IEEE Access 6, 46833–46843.

Wu, W., He, Y., Blaabjerg, F., 2012. An LLCL power filter for single-phase grid-tied inverter. IEEE Trans. Power Electron. 27 (2), 782–789.

Xu, J., Xie, S., Tang, T., 2013. Evaluations of current control in weak grid case for grid-connected LCL-filtered inverter. IET Power Electron. 6 (2), 227–234.

Xu, J., Yang, J., Ye, J., et al., 2014. An LTCL filter for three-phase grid-connected converters. IEEE Trans. Power Electron. 29 (8), 4322–4338.

Yang, H., Qi, J., Miao, Y., 2019a. A new robot navigation algorithm based on a double-layer ant algorithm and trajectory optimization. IEEE Trans. Ind. Electron. 66 (11), 8557–8566.

Yang, J., Wang, X., P., Bauer., 2019b. Extended PSO based collaborative searching for robotic swarms with practical constraints. IEEE Access 7, 76328–76341.

Yang, G., Zhou, F., Ma, Y. others, 2018. Identifying lightning channel-base current function parameters by Powell particle swarm optimization method. IEEE Trans. Electromagn. Compat. 60 (1), 182–187.

Ye, J., A., Shen., Zhang, Z., et al., 2018. Systematic design of the hybrid damping method for three-phase inverters with high-order filters. IEEE Trans. Power Electron. 33 (6), 4944–4956.
Yin, Z., Du, C., Liu, J., et al., 2018. Research on auto disturbance-rejection control of induction motors based on an ant colony optimization algorithm. IEEE Trans. Ind. Electron. 65 (4), 3077–3094.
Zhang, Y.H., Gong, Y.J., Chen, W.N., et al., 2019. A dual-colony ant algorithm for the receiving and shipping door assignments in cross-docks. IEEE Trans. Intell. Transp. Syst. 20 (7), 2523–2539.
Zhang, H., Liang, Y., Zhang, W., et al., 2018. Improved PSO-based method for leak detection and localization in liquid pipelines. IEEE Trans. Ind. Inf. 14 (7), 3143–3154.